MACROSCOPIC AND MICROSCOPIC BLOOD FLOWS

Franck NICOUD[1,4], Salomé Bru[2], Pierre Pottier[2,3], Pierre Taraconat[3], Simon MENDEZ[2]

[1] Corresponding Author. Institut Montpeliérain Alexander Grothendieck, University of Montpellier, CNRS, Place Bataillon, 31095 Montpellier, France. Tel.: +33 6 730 55140, E-mail: franck.nicoud@umontpellier.fr
[2] Institut Montpeliérain Alexander Grothendieck, University of Montpellier, CNRS, Montpellier, France
[3] HORIBA Medical, 398 rue du Caducée - 34790 Grabels, France
[4] Institut Universitaire de France, Paris, France

ABSTRACT

This paper highlights some of the advancements enabled by computational physics in the field of cardiovascular biomechanics. We briefly introduce the numerical methods of the YALES2BIO platform before delving into two ongoing studies. The first study exemplifies macroscopic scenarios where blood is modelled as a continuous fluid. Specifically, we examine intracardiac hemodynamics, exploring how the design of the mitral valve can alter turbulent dissipation. This study demonstrates how such simulations can enhance a medical imaging technique used routinely in clinical settings. The second example addresses situations where the physical phenomena occur at such small scales that the suspension nature of blood must be considered. We discuss the results of a numerical pipeline designed to simulate the operation of an industrial blood cytometer, illustrating how computational physics can provide access to data that is experimentally unattainable and useful for improving system performance.

Keywords: cardiovascular biomechanics, computational physics, cardiac efficiency, red blood cells, cytometry

1. INTRODUCTION

The ability to predict blood flow characteristics could significantly enhance diagnostic and treatment capabilities, given that many cardiovascular diseases are related to blood flow features. In this respect, computational physics serves as a natural complement to theoretical, experimental, and medical imaging techniques used to address questions related to both microscopic and macroscopic blood flows.

Many medical questions related to blood flow pertain to the largest arteries and veins in the cardiovascular system. Typical length scales range from 1 mm to a few centimeters, and the Reynolds number can be as high as several thousand. At these scales, blood is often considered a homogeneous fluid with either constant viscosity (typically $\mu = 3 \times 10^{-3}$ Pa.s) or characterized by shear-thinning behavior. Key challenges include managing the highly complex and deformable geometry of the blood flow domain, the transitional nature of wall-bounded blood flow, interactions with thin and highly deformable membranes (e.g., valve leaflets), thrombus formation due to biomedical materials, and validation.

In reality, blood is not homogeneous but a dense suspension (volume fraction ranging from 20-50%) of particles sized from $2\,\mu m$ (platelets) to $20\,\mu m$ (white blood cells). Over 95% of the cells flowing in plasma are red blood cells, which are non-spherical particles (equivalent diameter of $6\,\mu m$). Given their reduced volume of only 0.65, red blood cells are highly deformable, with their dynamics resulting from the coupling between the inner fluid (cytosol), the cell membrane, and the outer fluid (plasma). In flow regimes typical of the microcirculation, hemodynamics is dominated by suspension-related phenomena, such as the non-inertial migration of red blood cells towards the center of vessels.

This paper outlines some of the accomplishments and ongoing modelling efforts utilizing the YALES2BIO solver (imag.umontpellier.fr/~yales2bio/), developed at Institut Montpelliérain Alexander Grothendieck (IMAG) in Montpellier, France. Section 2 provides a brief overview of the numerical strategy employed. Section 3 illustrates how macroscopic simulations of intracardiac flow can enhance a medical imaging technique, specifically echocardiography, and deepen the overall understanding of cardiac function. Section 4 presents the results of a numerical pipeline designed to simulate the dynamics of red blood cells flowing through a Coulter-based cytometer,

demonstrating its potential to improve the cytometer's performance.

2. NUMERICAL METHOD

YALES2BIO is a highly parallelized multiphysics solver, derived from the YALES2 solver developed at CORIA in Rouen, France. It is specifically designed for simulating blood flows at both macroscopic and microscopic scales. At its core, YALES2BIO solves the incompressible Navier-Stokes equations using a finite-volume approach with a fourth-order discretization scheme, suitable for unstructured meshes [1]. To maintain the divergence-free property of the velocity field, the solver employs the projection method introduced by Chorin [2]. Namely, the velocity field is first advanced in time using a low-storage, fourth-order Runge-Kutta scheme [3] during a prediction step. This predicted velocity field is then corrected by applying a pressure gradient, which is obtained by solving a Poisson equation for pressure. The Poisson equation is solved using the Deflated Preconditioned Conjugate Gradient algorithm [4]. For turbulence modeling, YALES2BIO performs large-eddy simulations using the sigma subgrid scale model [5, 6]. This model ensures that no eddy viscosity is applied in canonical laminar flows and is well-suited for wall-bounded and transitional flows [7, 8]. Additionally, the solver can handle computations with moving meshes by employing an Arbitrary Lagrangian-Eulerian formulation [9, 10].

YALES2BIO conducts various simulations involving fluid-structure interactions at both macroscopic [11] and microscopic scales [12-14]. For fluid-structure coupling, the solver utilizes Peskin's immersed boundary method (IBM) for massless structures [15]. In this approach, the fluid perceives the structure's action as a force density applied during the prediction step. The forced Navier-Stokes equations are then solved as previously described. Once the flow velocity is computed, the structure is convected by the flow after interpolating the fluid velocity onto the structure.

Since the deformed structure is massless, it remains in equilibrium, allowing for the calculation of forces at the nodes of the structure mesh. These forces are then regularized, or spread, over the fluid mesh. As YALES2BIO employs unstructured meshes, the original IBM, designed for Cartesian meshes, has been adapted using the Reproducing Kernel Particle Method. This method ensures that force regularization and velocity interpolation impose several mathematical moments of the regularization/interpolation function [16-18]. For red blood cells (RBCs), the membrane mechanics are modeled by combining different models that represent either the in-plane [19] or out-of-plane resistances of the membrane [20]. More details may be found in Mendez and Abkarian [14]. The method, initially developed for infinitely thin membranes, has also been extended to finite-size yet thin structures [11, 21].

Numerous validation test cases have been presented in both 2D [18] and 3D [21], particularly for fluid-structure interaction coupling. The remainder of this paper describes two ongoing applications to illustrate how computational physics can address academic, medical, or industrial questions relevant to either macroscopic (Section 3) or microscopic (Section 4) scales.

3. INTRACARDIAC BLOOD FLOW

Chnafa et al. utilized YALES2BIO to simulate intracardiac flow that aligns with the time-evolving geometry observed through computed tomography of an actual patient [9] or magnetic resonance imaging of a normal volunteer [10]. In both scenarios, the computational domain spans from the four pulmonary veins to the root of the aorta, encompassing the left atrium and ventricles, as well as simplified models of the mitral and aortic valves.

The simulations employed Large Eddy Simulations based on a subgrid scale model well-suited for representing wall-bounded transitional flows [5, 22], and were conducted over more than 50 cardiac cycles. The analysis revealed that turbulence is periodically generated in the left ventricle at the end of diastole and dissipates during systole [23]. Moreover, the large vortex observed from advanced medical imaging techniques [24] during late diastole is accurately captured in the phase-averaged computational results. This particular flow feature is of significant medical interest, as it is believed to aid in redirecting blood momentum towards the ventricle's outlet, thereby facilitating ejection. For cardiologists, the ability to characterize this feature using routine echocardiography would be highly beneficial.

To achieve this, it is essential to reconstruct the intraventricular velocity field based on the radial component measured in colour Doppler mode. The numerical database for intraventricular flow [9] has been instrumental in developing a reconstruction algorithm based on an optimization procedure [25]. As illustrated in Figure 1, the Computational Fluid Dynamics (CFD) recirculation zone is well retrieved by the so-called intraventricular Vector Flow Mapping (iVFM) technique. Several enhancements to the original algorithm have been proposed to better incorporate the divergence-free constraint [26] and to represent the three-dimensional structures of the flow more accurately [27]. Recently, a methodology based on machine learning has proven to be both robust and efficient in retrieving intraventricular flow features from echocardiography [28]; a physics-guided neural network was trained using a database produced at IMAG, which included a variety of sizes, heart rates, and mitral valve designs [29].
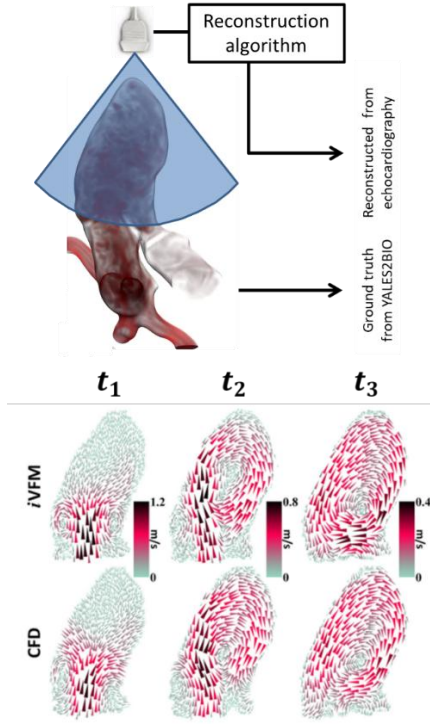
2

Figure 1. Top: A virtual echocardiography exam is performed on the numerical intracardiac flow. Bottom: The flow structure reconstructed from the virtual echocardiography image (top) is compared to the exact flow structure from the numerical database (bottom) at three different time points.

In addition to supporting the development of reconstruction methods for echocardiography, detailed simulations of intracardiac flow can enhance the overall understanding of heart function. As previously mentioned, the large vortex observed through advanced medical imaging techniques [24] during late diastole is of particular medical interest. It is believed to help redirect blood momentum toward the ventricle's outlet, thereby facilitating ejection [30]. This mechanism and its implications for the heart's pumping efficiency were recently studied computationally using simulations similar to those conducted by Chnafa et al. [9] enriched by a parameterized model, allowing for the investigation of the mitral valve shape's effect on intraventricular flow. Four cases considered are illustrated in Figure 2, which displays the vortical structure of the intraventricular flow at late diastole.
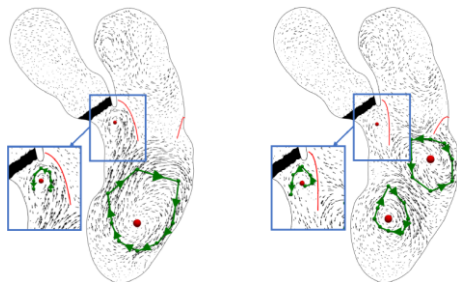

Figure 2. Phase-averaged velocity field at mid-diastole, the phase during which a large vortex, supposedly favourable for blood ejection through the aorta, is expected to be present. Green regions denote the different vortices within the ventricle, while red markers indicate their respective centres. The red lines depict the intersection between the mitral valve and the plane of view. Top left (C01): Physiological mitral valve with normal opening and orientation. Top right (C02): Normal opening with anterior orientation. Bottom left (C03): Normal orientation with wider opening. Bottom right (C04): Posterior orientation with smaller opening.

The expected large vortical structure is accurately captured in the reference case (top left), where the mitral valve opening and orientation are physiological. In cases where the valve opening is enlarged (bottom left) or reduced (bottom right), a vortical structure is still present, although its size and position are altered. The modifications are even more pronounced when the orientation of the mitral valve is changed (top right). In this scenario, the expected clockwise-rotating vortex (top left) is replaced by a pair of counter-rotating vortices. It is evident that the details of the mitral valve geometry significantly impact the flow organization within the ventricle.

To determine whether these modifications result in a significant change in cardiac pumping efficiency, the balance of ventricular kinetic energy has been recently studied [29]. This balance is obtained by integrating the kinetic energy equation over the time-dependent ventricular domain and applying the Reynolds transport theorem. The different contributions are displayed in Figure 3, which provides a physical interpretation of each term. In all the cases considered, the contributions sum up to approximately zero within a small fraction (approximately 3%) of the ventricle's power. This indicates that the simulations can be reliably used to further analyse the energy balance within the ventricle. As illustrated in Figure 4, this balance is dominated by the three pressure terms P_{AP}, P_{MP} and P_{muscle} (see Fig. 3), regardless of the specifics of the mitral valve.

$$-\iint_{MV} p\mathbf{u}\cdot\mathbf{n}\,dS \quad \text{Pressure force power } [P_{MP}]$$

$$-\iint_{AV} p\mathbf{u}\cdot\mathbf{n}\,dS \quad \text{Pressure force power } [P_{AP}]$$

$$\iint_{MV} \rho E_c \mathbf{u}\cdot\mathbf{n}\,dS \quad \text{Energy flux } [E_{MP}]$$

$$\iint_{AV} \rho E_c \mathbf{u}\cdot\mathbf{n}\,dS \quad \text{Energy flux } [E_{AP}]$$

$$\iiint_{MV} \rho \mathbf{F}\cdot\mathbf{u}\,dV \quad \text{MV power } [MV]$$

$$\iiint_{Vent} 2(\mu + \mu_{SGS})\mathbf{S}:\mathbf{S}\,dV \quad \text{Dissipation } [\psi]$$

$$\frac{d}{dt}\iiint_{Vent} \rho E_c\,dV \quad \text{Energy storage}$$

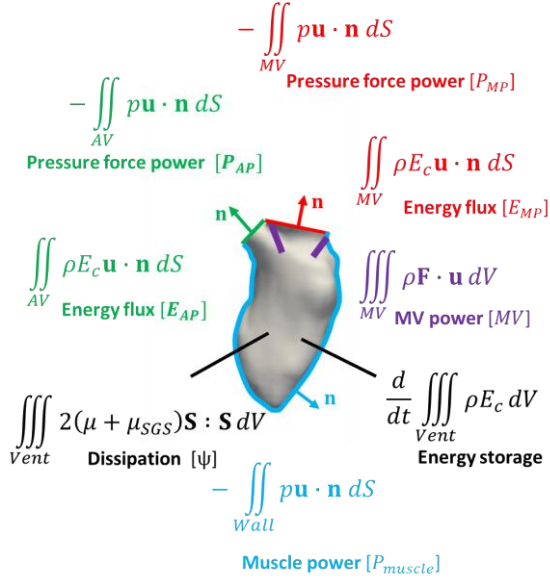$$-\iint_{Wall} p\mathbf{u}\cdot\mathbf{n}\,dS \quad \text{Muscle power } [P_{muscle}]$$

Figure 3. Main contributions to the balance of kinetic energy within the control volume defined by the cardiac muscle (blue) and two fixed planes located near the mitral annulus (red) and the aortic valve (green). In addition to energy storage (which cancels out after time integration due to time periodicity of the cardiac cycle), the two volume terms include the power of the mitral valve leaflets (violet) and the viscous dissipation (black). The latter accounts for turbulent effects through subgrid scale viscosity μ_{SGS}.

However, the dissipation term is highly dependent on the valve opening, reaching a value three times larger when the valve opens less (case C04) compared to the wider opening (case C03) — see Figure 4. Despite this variation, the amount of energy dissipated over one cardiac cycle remains a small fraction (1-2%) of the energy involved in pumping blood from the atrium to the aorta. From this perspective, the energy efficiency of the pumping mechanism remains very high (greater than 98%), independent of the mitral valve design and flow structure within the ventricle. Note that this conclusion may not hold in cases where valve leakage is present, causing some blood to flow back into the atrium during systole.
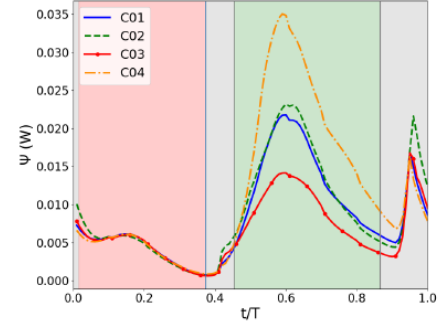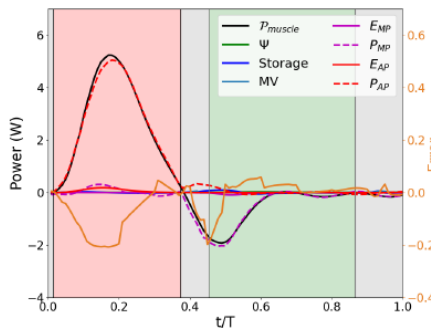

Figure 4. The top plot illustrates the time evolution of the main contributors to the kinetic energy balance for the normal case C01. The acronyms are defined in Figure 3. Very similar evolutions are obtained for the other cases displayed in Figure 2 (not shown). The bottom plot shows the time evolution of the dissipation term.

4. COMPUTATIONAL CYTOMETRY IMAGING

Taraconat et al. [31] examined the impedance measurement of red blood cells (RBCs) in an industrial hematology analyzer. The setup consists of a polarized micro-orifice through which red blood cells are aspirated one at a time, as illustrated in Figure 5. This constriction ensures a high electrical field in the aperture, such that the presence of an RBC increases the electrical resistance, detectable as a voltage pulse. Counting these electrical signals provides a tally of cells passing through the micro-orifice, and the amplitudes of these perturbations are assumed to be proportional to the particle sizes [32]. Commonly known as 'Coulter counter' [33], this system measures RBC volumes and concentrations. Although Coulter counters have been integral to blood analyzers for decades, some measurement artifacts remain poorly understood. Near the aperture walls, inhomogeneities in the electrical field and complex RBC dynamics lead to measurement errors. Investigating particle dynamics in the detection area to understand these edge effects is challenging due to accessibility issues in industrial systems. Consequently, numerical simulation was chosen as the preferred method for these investigations.
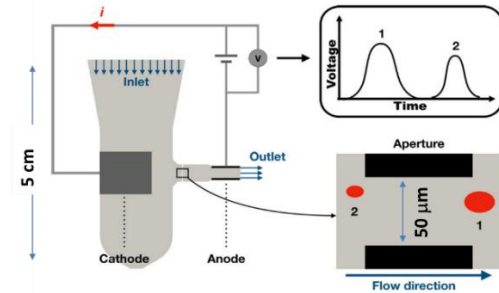

4

Figure 5. Principle of counting and sizing (red blood) cells using a Coulter counter. The diluted blood sample flows into the tank through the inlet, and each circulating cell generates an electrical perturbation, supposedly proportional to its volume, as it passes through the aperture. The cells then exit the system through the outlet. Note the significant separation of scales between the tank (cm) and the cell (μm) size.

Simulating deforming cells in a Coulter counter presents a multi-scale challenge that has been addressed through a specific sequence of simulations [31]. Essentially, the flow domain is conceptually divided into three distinct parts, each requiring a different type of simulation to accurately represent the physical phenomena occurring within them.

1. **Passive Transport Region**: In the largest part of the domain, red blood cells (RBCs) behave like passive tracers. They are transported by the flow without undergoing deformation.
2. **Stretching Region**: In an intermediate region, the RBCs continue to follow the streamlines of the baseline flow but begin to stretch as they move.
3. **Deformation and Rotation Region**: Finally, as the RBCs flow through the micro-orifice, they experience deformation and may rotate, thereby disturbing the electrical field.

The varying durations of these phases—on the order of 50 seconds, 20 milliseconds, and 20 microseconds, respectively—highlight the multi-scale complexity inherent in this type of analysis. The numerical simulation of the electrical pulse, which corresponds to the experimental measurements taken during each cell passage, is computed under static conditions. This involves solving the Laplace equation for the electrical potential across a series of cell positions and shapes.

The proposed simulation method was benchmarked against experimental data derived from both healthy blood samples and latex bead samples. Figure 6 demonstrates that the numerical results not only replicate the experimental findings but also offer deeper insights into the complex behaviors observed when particles traverse near the wall regions.

Specifically, the analysis reveals two distinct types of edge effects:

1. **Electrical Edge Effects**: These occur when particles pass through areas with highly non-uniform electrical fields, particularly near the corners of the aperture. This phenomenon is visually indicated by blue circles in Figure 6. The non-uniformity in the electrical field leads to variations in the electrical signals detected.

2. **Dynamical Edge Effects**: These involve the rotation of cells induced by significant velocity gradients near the aperture walls, as shown by black arrows in Figure 6. The shear forces in these regions cause the cells to rotate, which in turn affects their orientation and the resulting electrical signatures.

The simulations effectively distinguish between these two types of artifacts, providing a clearer understanding of their individual impacts on the electrical measurements. This separation is crucial for accurately interpreting the data obtained from Coulter counters and improving the precision of blood analysis techniques.
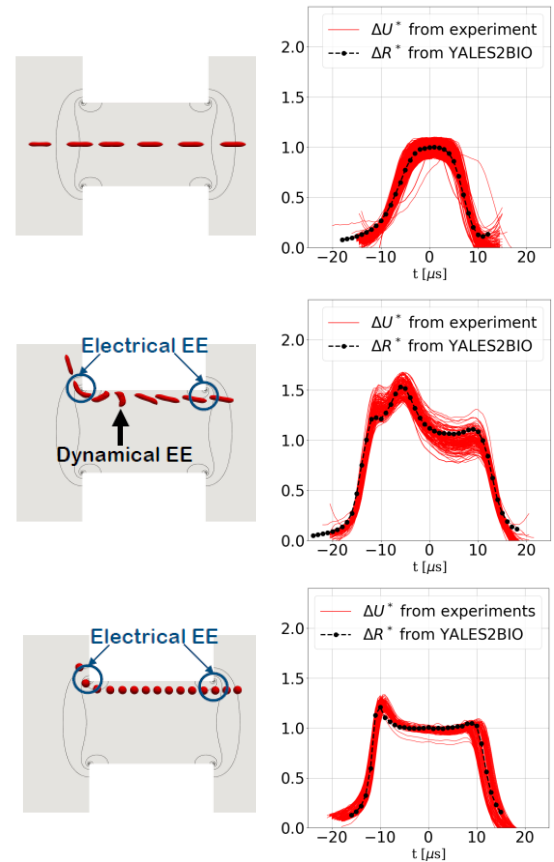

Figure 6. The left column illustrates the simulated dynamics of red blood cells (RBCs) in the micro-orifice, while the right column displays the associated electrical perturbations. In the right column, electrical pulses derived from simulations are superimposed with experimental observations. The top, middle, and bottom rows correspond to an RBC on a centred trajectory, an RBC on a near-wall trajectory, and a rigid sphere on a near-wall trajectory, respectively. Electrical field isolines are shown over the cut view of the fluid domain in the particle dynamics images of the left column. Electrical and dynamical edge effects (EE) are highlighted by blue circles and black arrows, respectively.

The cell rotation that occurs for cells flowing close to the wall of the aperture artificially increases the shape factor of the cell and thus the amplitude of the electrical perturbation [32]. This explains the right-skewed probability density function of the cells volume often observed in practice. Leveraging this knowledge and a numerical database built from the numerical pipeline developed in [31], two strategies were recently proposed [34] and patented [35] to correct the sizing error in Coulter-based cytometry. These strategies are based either on signal processing of the electrical pulse or on a neural network capable of detecting whether the cell has experienced rotation. Detecting and rejecting rotation-associated pulses have been shown to provide results comparable to hydrodynamic focusing [36], which forces cells to flow in the centre of the orifice, the gold standard implementation of the Coulter principle.

In the computational studies cited above, the membrane of red blood cells was modeled as purely hyperelastic, despite experimental evidence indicating viscoelastic behavior. Enhancing the physical description of membrane rheology [37] provides an even more accurate description of cell dynamics as they flow through the apparatus [38]. This improvement paves the way for Coulter-based detection of cellular pathologies.

5. DISCUSSION

Computational physics is now recognized as a complementary tool that, alongside experimental and theoretical approaches, can provide relevant answers to practical blood-related questions. This paper has discussed two examples, focusing on macroscopic intracardiac flow and the counting and sizing of red blood cells.

Over the past years, many other applications and scientific questions have been addressed at IMAG. On the macroscopic side, notable studies include the interaction between turbulent flow and aortic [21] or venous [39] valves, he robustness of computational representations of jet-like flows such as in the Food and Drug Administration cannula test case [40], and the modelling of intra-vascular medical devices like flow diverters or WEBs [41, 42]. Regarding the microscopic scales, successful studies have been conducted on the dynamics of a single red blood cell in shear flow [13], which have been compared to theoretical [43] and experimental [44] data, as well as the self-organization of cells in a microfluidic channel [45]. Modelling the thrombosis phenomenon requires both macroscopic [46, 47] and microscopic [48] computational capabilities, as well as a reliable and efficient description of the biochemical reactions involved in the coagulation cascade [49-51]. As a final note, let us mention a recent and active research topic at IMAG where computational physics is used to mimic the medical images obtained from actual Magnetic Resonance Imaging systems [52]. This aims to better understand the limitations and optimize the sequences used in clinical routines [53].

REFERENCES

[1] V. Moureau, P. Domingo, and L. Vervisch, "Design of a massively parallel CFD code for complex geometries," *Comptes Rendus Mécanique*, vol. 339, no. 2–3, pp. 141–148, 2011, doi: 10.1016/j.crme.2010.12.001.

[2] A. Chorin, "Numerical solution of the Navier-Stokes equations," *Math. Comput.*, vol. 22, pp. 745–762, 1968, doi: 10.2307/2004575.

[3] V. Moureau, P. Domingo, and L. Vervisch, "From Large-Eddy Simulation to Direct Numerical Simulation of a lean premixed swirl flame: Filtered laminar flame-PDF modeling," *Combust. Flame*, vol. 158, no. 7, pp. 1340–1357, 2011, doi: 10.1016/j.combustflame.2010.12.004.

[4] M. Malandain, N. Maheu, and V. Moureau, "Optimization of the deflated Conjugate Gradient algorithm for the solving of elliptic equations on massively parallel machines," *J. Comput. Phys.*, vol. 238, pp. 32–47, 2013, doi: 10.1016/j.jcp.2012.11.046.

[5] F. Nicoud, H. Baya Toda, O. Cabrit, S. Bose, and J. Lee, "Using singular values to build a subgrid-scale model for large eddy simulations," *Phys. Fluids*, vol. 23, no. 8, p. 085106, 2011, doi: 10.1063/1.3623274.

[6] H. B. Toda, O. Cabrit, K. Truffin, G. Bruneaux, and F. Nicoud, "Assessment of subgrid-scale models with a large-eddy simulation-dedicated experimental database: The pulsatile impinging jet in turbulent cross-flow," *Phys. Fluids*, vol. 26, no. 7, 2014, doi: 10.1063/1.4890855.

[7] F. Nicoud, C. Chnafa, J. Siguenza, V. Zmijanovic, and S. Mendez, "Large-Eddy simulation of turbulence in cardiovascular flows," in *Lecture Notes in Applied and Computational Mechanics*, vol. 84, Peter Wriggers \& Thomas Lenarz, Ed., Springer, Cham, 2018, pp. 147–167. doi: 10.1007/978-3-319-59548-1_9.

[8] F. Nicoud, M. Garreau, and S. Mendez, "Turbulence modeling of blood flow," in *Biomechanics of the Aorta*, C. Gasser, S. Avril, and J. Elefteriades, Eds., Academic Press, 2024, pp. 387–414. doi: 10.1016/B978-0-323-95484-6.00010-5.

[9] C. Chnafa, S. Mendez, and F. Nicoud, "Image-based large-eddy simulation in a realistic left heart," *Comput. Fluids*, vol. 94, pp. 173–187, 2014, doi: 10.1016/j.compfluid.2014.01.030.

[10] C. Chnafa, S. Mendez, and F. Nicoud, "Image-Based Simulations Show Important Flow Fluctuations in a Normal Left Ventricle: What Could be the Implications?," *Ann. Biomed. Eng.*, vol. 44, no. 11, pp. 3346–3358, 2016, doi: 10.1007/s10439-016-1614-6.

[11] J. Sigüenza *et al.*, "Validation of an immersed thick boundary method for simulating fluid–structure interactions of deformable membranes," *J. Comput. Phys.*, vol. 322, pp. 723–746, 2016, doi: 10.1016/j.jcp.2016.06.041.

[12] L. Lanotte *et al.*, "Red cells' dynamic morphologies govern blood shear thinning under microcirculatory flow conditions," *Proc. Natl. Acad. Sci.*, vol. 113, no. 47, pp. 13289–13294, 2016, doi: 10.1073/pnas.1608074113.

[13] J. Mauer *et al.*, "Flow-Induced Transitions of Red Blood Cell Shapes under Shear," *Phys. Rev. Lett.*, vol. 121, no. 118103, pp. 1–6, 2018, doi: 10.1103/PhysRevLett.121.118103.

[14] S. Mendez and M. Abkarian, "Single red blood cell dynamics in shear flow and its role in hemorheology," in *Dynamics of Blood Cell Suspensions in Microflows*, Taylor and Francis Group, 6000 Broken Sound Parkway NW, Suite 300, Boca Raton, FL 33487-2742: CRC Press., 2019, pp. 125–182. doi: 10.1201/b21806-5.

[15] C. Peskin, "The immersed boundary method," *Acta Numer.*, vol. 11, pp. 479–517, 2002, doi: 10.1017/S0962492902000077.

[16] W. K. Liu, S. Jun, and Y. F. Zhang, "Reproducing kernel particle methods," *Int. J. Numer. Methods Fluids*, vol. 20, no. 8–9, pp. 1081–1106, Apr. 1995, doi: 10.1002/FLD.1650200824.

[17] A. Pinelli, I. Naqavi, U. Piomelli, and J. Favier, "Immersed-boundary methods for general finite-difference and finite-volume Navier-Stokes solvers," *J. Comput. Phys.*, vol. 229, no. 24, pp. 9073–9091, 2010, doi: 10.1016/j.jcp.2010.08.021.

[18] S. Mendez, E. Gibaud, and F. Nicoud, "An unstructured solver for simulations of deformable particles in flows at arbitrary Reynolds numbers," *J. Comput. Phys.*, vol. 256, pp. 465–483, 2014, doi: 10.1016/j.jcp.2013.08.061.

[19] R. Skalak, A. Tozeren, R. Zarda, and S. Chien, "Strain energy function of red blood cell membranes," *Biophys. J.*, vol. 13, pp. 245–264, 1973, doi: 10.1016/S0006-3495(73)85983-1.

[20] W. Helfrich, "Elastic properties of lipid bilayers: Theory and possible experiments.," *Z Naturforsch*, vol. 28, pp. 693–703, 1973, doi: 10.1515/znc-1973-11-1209.

[21] J. Sigüenza *et al.*, "Fluid-structure interaction of a pulsatile flow with an aortic valve model: A combined experimental and numerical study," *Int. j. numer. method. biomed. eng.*, vol. 34, no. 4, pp. 1–19, 2018, doi: 10.1002/cnm.2945.

[22] H. Baya Toda, O. Cabrit, K. Truffin, G. Bruneaux, and F. Nicoud, "Assessment of subgrid-scale models with a large-eddy simulation-dedicated experimental database: The pulsatile impinging jet in turbulent cross-flow," *Phys. Fluids*, vol. 26, no. 7, p. 075108, 2014, doi: 10.1063/1.4890855.

[23] C. Chnafa, S. Mendez, R. Moreno, and F. Nicoud, "Using image-based CFD to investigate the intracardiac turbulence," in *Modeling the Heart and the Circulatory System. MS&A Vol. 14*, A. Quarteroni, Ed., New-York: Springer International Publishing, 2015, pp. 97–117. doi: 10.1007/978-3-319-05230-4_4.

[24] M. Markl, P. Kilner, and T. Ebbers, "Comprehensive 4D velocity mapping of the heart and great vessels by cardiovascular magnetic resonance.," *J. Cardiovasc. Magn. Reson.*, vol. 13, no. 1, p. 7, 2011, doi: 10.1186/1532-429X-13-7.

[25] K. C. Assi *et al.*, "Intraventricular vector flow mapping - A Doppler-based regularized problem with automatic model selection," *Phys. Med. Biol.*, vol. 62, no. 17, pp. 7131–7147, Aug. 2017, doi: 10.1088/1361-6560/aa7fe7.

[26] F. Vixege *et al.*, "Physics-constrained intraventricular vector flow mapping by color Doppler," *Phys. Med. Biol.*, vol. 66, p. 245019, Dec. 2021, doi: 10.1088/1361-6560/ac3ffe.

[27] F. Vixege *et al.*, "Full-volume three-component intraventricular vector flow mapping by triplane color Doppler," *Phys. Med. Biol.*, vol. 67, no. 9, 2022, doi: 10.1088/1361-6560/ac62fe.

[28] H. J. Ling *et al.*, "Physics-Guided Neural Networks for Intraventricular Vector Flow Mapping," *IEEE Trans. Ultrason. Ferroelectr. Freq. Control*, vol. 71, no. 11, pp. 1377–1388, 2024, doi: 10.1109/TUFFC.2024.3411718.

[29] F. Nicoud, S. Bru, and S. Mendez, "Realistic intracardiac hemodynamics: A computational study," in *12th FIMH conference – (Lyon, France)*, 2023.

[30] P. Kilner, G. Yang, J. Wilkes, R. Mohiaddin, D. Firmin, and M. Yacoub, "Asymmetric redirection of flow through the heart.," *Nature*, vol. 404, no. 6779, pp. 759–761, 2000, doi: 10.1038/35008075.

[31] P. Taraconat, J.-P. Gineys, D. Isèbe, F. Nicoud, and S. Mendez, "Numerical simulation of deformable particles in a Coulter counter," *Int. j. numer. method. biomed. eng.*, vol. 35, no. 11, p. e3243, 2019, doi: 10.1002/cnm.3243.

[32] V. Kachel, "Electrical resistance pulse sizing: Coulter sizing," in *Flow cytometry and sorting*, 1990, pp. 45–80.

[33] W. H. Coulter, "Means for counting particles

suspended in a fluid," 1953

[34] P. Taraconat, J.-P. Gineys, D. Isèbe, F. Nicoud, and S. Mendez, "Detecting cells rotations for increasing the robustness of cell sizing by impedance measurements , with or without machine learning," *Cytometry*, vol. 99, no. 10, pp. 977–986, 2021, doi: 10.1002/cyto.a.24356.

[35] P. Taraconat, D. Isebe, F. Nicoud, and S. Mendez, "Focalisation numérique pour le tri des signaux d'impédance Coulter et l'amélioration de la volumétrie des cellules - Patent #FR1904410 - WO/2020/216952," FR1904410-WO/2020/216952, 2019

[36] L. Spielman, "Improving resolution in Coulter counting by hydrodynamic focusing," *J Colloid Interface Sci.*, vol. 26, pp. 175–182, 1968.

[37] P. Matteoli, F. Nicoud, and S. Mendez, "Impact of the membrane viscosity on the tank-treading behavior of red blood cells," *Phys. Rev. Fluids*, vol. 043602, pp. 1–21, 2021, doi: 10.1103/PhysRevFluids.6.043602.

[38] P. Pottier, P. Taraconat, J.-P. Gineys, D. Isèbe, F. Nicoud, and S. Mendez, "Key role of red blood cell membrane viscosity in Coulter counter signal understanding," in *12th International Conference on Multiphase Flow, Toulouse, France*, 2025.

[39] B. Thibaud, I. Soler, S. Mendez, and F. Nicoud, "Fluid-structure interaction modeling of deep vein valves," in *7th International Conference on Computational and Mathematical Biomedical Engineering*, Milan, 2022.

[40] V. Zmijanovic, S. Mendez, V. Moureau, and F. Nicoud, "About the Numerical Robustness of Biomedical Benchmark Cases: Interlaboratory FDA's Idealized Medical Device," *Int. j. numer. method. biomed. eng.*, vol. 33, no. 1, pp. 1-17 e02789, 2017, doi: 10.1002/cnm.2789.

[41] A. Bérod, C. Chnafa, S. Mendez, and F. Nicoud, "A Heterogeneous Model of Endovascular Devices for the Treatment of Intracranial Aneurysms," *Int. j. numer. method. biomed. eng.*, vol. 38, no. 2, p. e3552, 2021, doi: 10.1002/cnm.3552.

[42] A. Bérod, F. Mut, J. Cebral, C. Chnafa, and F. Nicoud, "Assessing a heterogeneous model for accounting for endovascular devices in hemodynamic simulations of cerebral aneurysms," *Int. j. numer. method. biomed. eng.*, no. June 2022, pp. 1–17, 2023, doi: 10.1002/cnm.3762.

[43] S. Mendez and M. Abkarian, "In-plane elasticity controls the full dynamics of red blood cells in shear flow," *Phys. Rev. Fluids*, vol. 3, no. 10, pp. 1–10, 2018, doi: 10.1103/PhysRevFluids.3.101101.

[44] L. Lanotte *et al.*, "Red cells' dynamic morphologies govern blood shear thinning under microcirculatory flow conditions," *Proc. Natl. Acad. Sci. U. S. A.*, vol. 113, no. 47, 2016,

doi: 10.1073/pnas.1608074113.

[45] C. Iss *et al.*, "Self-organization of red blood cell suspensions under confined 2D flows," *Soft Matter*, vol. 15, pp. 2971–2980, 2019, doi: 10.1039/C8SM02571A.

[46] R. Méndez Rojano, S. Mendez, and F. Nicoud, "Introducing the pro-coagulant contact system in the numerical assessment of device-related thrombosis," *Biomech. Model. Mechanobiol.*, vol. 17, no. 3, pp. 815–826, 2018, doi: 10.1007/s10237-017-0994-3.

[47] R. Mendez Rojano *et al.*, "Kinetics of the coagulation cascade including the contact activation system : Sensitivity analysis and model reduction," *Biomech. Model. Mechanobiol.*, vol. 18, no. 4, pp. 1139–1153, 2019.

[48] C. Raveleau, S. Mendez, and F. Nicoud, "Impact of microstructured artificial surfaces on the dynamics of blood platelets," in *ESAO Congress, Enschede, The Netherlands*, 2025.

[49] F. Nicoud, "An adjoint-based method for the computation of gradients in coagulation schemes," *Int. j. numer. method. biomed. eng.*, vol. 39, no. 5, p. e3698, Mar. 2023, doi: 10.1002/cnm.3698.

[50] A. Ranc, S. Bru, S. Mendez, M. Giansily-Blaizot, F. Nicoud, and R. Mendez Rojano, "Critical evaluation of kinetic schemes for coagulation," *PLoS One*, vol. 18, no. 8, p. e0290531, 2023, doi: 10.1371/journal.pone.0290531.

[51] J. Chen, Q. Cazères, E. Riber, and F. Nicoud, "Multistep model reduction of coagulation schemes," *Biomech. Model. Mechanobiol.*, vol. 24, pp. 919–937, 2025, doi: 10.1007/s10237-025-01944-9.

[52] T. Puiseux, A. Sewonu, R. Moreno, S. Mendez, and F. Nicoud, "Numerical simulation of time-resolved 3D phase-contrast magnetic resonance imaging," *PLoS One*, vol. 16, no. 3, p. e0248816., 2021, doi: 10.1371/journal.pone.0248816.

[53] M. Garreau *et al.*, "Accelerated sequences of 4D flow MRI using GRAPPA and compressed sensing : A comparison against conventional MRI and computational fluid dynamics," *Magn. Reson. Imaging*, no. June, pp. 1–15, 2022, doi: 10.1002/mrm.29404.